RSC Advances

PAPER

View Article Online
View Journal | View Issue

Check for updates

Cite this: *RSC Adv.*, 2020, **10**, 42021

Reversible electrodeposition and stripping of magnesium from solvate ionic liquid–tetrabutylammonium chloride mixtures†

Pieter Geysens, [a] Jan Fransaer [b] and Koen Binnemans *[a]

Received 24th September 2020
Accepted 9th November 2020

DOI: 10.1039/d0ra08187f

rsc.li/rsc-advances

The physicochemical properties of three new magnesium-containing solvate ionic liquids are reported. The solvation structures were analysed by Raman spectroscopy, revealing a solvent separated ion pair structure at room temperature. The reversible electrodeposition and stripping of magnesium from mixtures of these solvate ionic liquids and tetra-*n*-butylammonium chloride is described. The electrolytes are significantly less volatile than similar dilute electrolytes, even at elevated temperatures and the deposition current densities exceed 1 A dm^{-2} at 80 °C. The influence of the chloride concentration on magnesium deposition was studied with cyclic voltammetry and chronopotentiometry. It was found that the stripping of magnesium is governed by two competing reactions, and the addition of tetrabutylammonium chloride to the solvate ionic liquids was necessary to prevent passivation and efficiently strip the deposited magnesium.

Open Access Article. Published on 18 November 2020. Downloaded on 12/6/2025 10:29:05 AM.
This article is licensed under a Creative Commons Attribution-NonCommercial 3.0 Unported Licence.

Introduction

Multivalent metals are being explored as an anode material for secondary batteries due to their high theoretical specific capacity.[1] Particularly, magnesium is of interest, as it is a highly abundant element and combines a very negative standard reduction potential (−2.38 V *versus* SHE) with a high volumetric capacity (3833 mA h cm^{-3}), resulting in a high theoretical energy density.[2] Furthermore, magnesium is less reactive than lithium and sodium, and it does not have the tendency to form dendritic deposits, making it an inherently safer anode material.[3,4] The main issue with magnesium metal anodes in rechargeable batteries is their tendency to form non-conductive surface films by reacting with organic electrolytes and trace impurities.[5,6]

For a long time, the only electrolytes that prevented formation of passivating films and allowed for reversible magnesium deposition consisted of Grignard reagents dissolved in ether solvents.[7] However, these electrolytes are unsuitable for use in batteries due to their high reactivity, poor anodic stability and safety issues.[8] By reacting Grignard reagents with Lewis acids such as boranes and haloaluminates, the anodic stability is significantly improved but the reactivity of these derivatives is still too high for actual battery use.[9–12]

More recently, a new class of fully inorganic electrolytes for reversible magnesium electrodeposition has emerged.[13,14] These are not derived from Grignard reagents and are more convenient for use in batteries. In particular, promising results were obtained with solutions of magnesium bis(trifluoromethylsulfonyl)imide ($Mg(Tf_2N)_2$) and a chloride salt in ether solvents.[15–18] While these electrolytes have a wide electrochemical window of approx. 3.5 V, and enable highly reversible magnesium electrodeposition at sizeable current density, the used solvents, tetrahydrofuran (THF) or 1,2-dimethoxyethane (DME, monoglyme, G1), are volatile and pose environmental and safety risks. Therefore, interest in less volatile electrolytes based on ionic liquids (ILs) has increased.[19,20] However, ionic liquids often have poor solvating properties towards metal salts, leading to low solubilities and as a consequence low deposition current densities.

Solvate ionic liquids (SILs), sometimes also called liquid metal salts (LMS), are a type of ILs where the cation consists of a metal ion, solvated by neutral ligands.[21] They overcome the solubility problem by integrating the metal in the IL structure, while also having a low volatility because the ligands are strongly coordinated to the metal cations. Lithium- and sodium-based SILs with oligo(ethylene glycol) dimethyl ethers (glymes) as ligands have been extensively investigated as safer alternative electrolytes for lithium,[22] lithium-ion[23,24] and sodium-ion[25,26] batteries. Two magnesium-based SILs have been reported, namely $[Mg(G3)][Tf_2N]_2$ (G3 = triglyme)[27,28] and

[a]*Department of Chemistry, KU Leuven, Celestijnenlaan 200F, P.O. Box 2404, B-3001 Leuven, Belgium. E-mail: Koen.Binnemans@kuleuven.be*

[b]*Department of Materials Engineering, KU Leuven, Kasteelpark Arenberg 44, B-3001 Leuven, Belgium*

† Electronic supplementary information (ESI) available: Raman spectra of $[Mg(G1)_3][Tf_2N]_2$ + pure G1 + pure $Mg(Tf_2N)_2$, and $[Mg(G3)_2][Tf_2N]_2$ + pure G3 + pure $Mg(Tf_2N)_2$. CVs of $[Mg(G1)_3][Tf_2N]_2$: TBACl 1 : 1, and $[Mg(G3)_2][Tf_2N]_2$: TBACl 1 : 1, measured against a Mg pseudo-RE. CVs of $[Mg(G3)_2][Tf_2N]_2$: TBACl 1 : 1, recorded on different WEs. Charge *vs.* time plots accompanying the CVs in Fig. 6a. CVs of $[Mg(G3)_2][Tf_2N]_2$: TBACl in different molar ratios, measured against a Mg pseudo-RE. See DOI: 10.1039/d0ra08187f

Open Access Article. Published on 18 November 2020. Downloaded on 12/6/2025 10:29:05 AM.
This article is licensed under a Creative Commons Attribution-NonCommercial 3.0 Unported Licence.

$[Mg(G4)][Tf_2N]_2$ (G4 = tetraglyme).[29] $[Mg(G3)][Tf_2N]_2$ and asymmetric analogues have low melting points (≤70 °C) and quasi-reversible magnesium deposition/stripping was achieved in these electrolytes. The electrochemistry of $[Mg(G4)][Tf_2N]_2$ was not investigated in detail due to its high melting point (137 °C).

In this paper, three new magnesium-based solvate ionic liquids are described: $[Mg(G1)_3][Tf_2N]_2$, $[Mg(G2)_2][Tf_2N]_2$ and $[Mg(G3)_2][Tf_2N]_2$. Mixtures of these compounds and tetrabutylammonium chloride (TBACl) were studied as electrolytes for reversible magnesium electrodeposition at 80 °C. TBACl was chosen as a source of chloride anions for several reasons. First, we found that the use of inorganic chloride salts (*e.g.* LiCl, $MgCl_2$) resulted in mixtures with a very high viscosity, beyond what is considered practical for electrochemical experiments. In contrast, the use of TBACl resulted in a decreased viscosity compared to the pure SILs, which is advantageous to achieve good mass transport during electrodeposition. Secondly, it is well known that the TBA^+ cation is electrochemically stable against the highly negative reduction potentials of magnesium, sodium, and even lithium. Furthermore, the addition of TBACl to $Mg(AlCl_2R_2)_2$-based electrolytes was shown to significantly improve their ionic conductivity and overall electrochemical performance by increasing the total concentration of ionic species.[30] The influence of chloride on the magnesium deposition and stripping process in these SIL : TBACl mixtures was investigated by cyclic voltammetry and chronopotentiometry.

Experimental

Materials and synthesis

Magnesium bis(trifluoromethylsulfonyl)imide ($Mg(Tf_2N)_2$, 99.5%) was purchased from Solvionic (Toulouse, France) and was dried at 250 °C for 48 h on a vacuum line prior to use. 1,2-Dimethoxyethane (monoglyme, G1, 99.5%, anhydrous) and 1-methoxy-2-(2-methoxyethoxy)ethane (diglyme, G2, 99.5%, anhydrous) were purchased from Sigma-Aldrich (Diegem, Belgium) and were used as received. 1,2-Bis(2-methoxyethoxy) ethane (triglyme, G3, 99%) was purchased from Sigma-Aldrich (Diegem, Belgium) and dried prior to use on molecular sieves (4 Å, 8 to 12 mesh) which were purchased from Acros Organics (Geel, Belgium). The water content of the glymes was measured by a Mettler-Toledo C30S coulometric Karl Fischer titrator and was found to be lower than 50 ppm, as claimed by the manufacturer. Tetra-*n*-butylammonium chloride (TBACl, ≥97%) was purchased from Sigma-Aldrich (Diegem, Belgium) and was dried at 110 °C for 48 h on a vacuum line prior to use. Ferrocenium hexafluorophosphate ($FcPF_6$, 97%) was purchased from Sigma Aldrich (Diegem, Belgium) and was used as received. Ferrocene (Fc, purum, ≥98%) was purchased from Fluka (Bucharest, Romania) and was used as received. *N*-Butyl-*N*-methylpyrrolidinium bis(trifluoromethylsulfonyl)imide ([BMP][Tf_2N], 99%) was purchased from Iolitec (Heilbronn, Germany) and was dried at 110 °C for 48 h on a vacuum line prior to use. Storage of the reagents and all the manipulations involving contact of the chemicals with the atmosphere were performed in an argon-filled glovebox with an oxygen and water concentration below 1 ppm. The solvate ionic liquids were prepared by adding a stoichiometric amount of glyme to $Mg(Tf_2N)_2$ in glass vials, which were closed with airtight screw caps afterwards, and subsequently heating the mixture under stirring until a homogeneous liquid was obtained. The liquids were then allowed to cool down to ambient glovebox temperature (~28 °C). The 1 : 1 mixtures SIL : TBACl were prepared in a similar way from the pure SILs and TBACl in the correct stoichiometric ratio. The mixtures were stirred under heating until homogeneous. Upon cooling, they (partially) crystallized out.

Methods

Melting points were determined on a Mettler-Toledo DSC-1 instrument at a heating rate of 10 °C min^{-1} under a helium atmosphere. Aluminium crucibles were filled with samples of electrolyte (3 to 12 mg) inside an argon-filled glovebox and sealed to prevent contact with the air. The samples were cycled twice (heating first) between −70 °C and 160 °C ([$Mg(G1)_3$][Tf_2N]$_2$ and $[Mg(G2)_2][Tf_2N]_2$) or 90 °C ($[Mg(G3)_2][Tf_2N]_2$). The melting point values determined in the second cycle are reported in Table 1. Thermogravimetric analysis (TGA) was performed on a TA Instruments TGA Q500 at a heating rate of 5 °C min^{-1} under a nitrogen atmosphere with a flow rate of 60 mL min^{-1}. The sample size was typically between 5 and 10 mg. In order to make the TGA traces of the different samples directly comparable, the data (mass *vs.* time) was normalized by dividing by their initial mass value. The data on the *y*-axis is expressed as the remaining fraction of the initial sample mass (in %). The viscosity and density of the electrolytes were

Table 1 Melting point, dynamic viscosity, density and Mg(II) concentration of pure complexes $[Mg(G1)_3][Tf_2N]_2$, $[Mg(G2)_2][Tf_2N]_2$ and $[Mg(G3)_2][Tf_2N]_2$ and 1 : 1 mixtures $[Mg(G1)_3][Tf_2N]_2$: TBACl and $[Mg(G3)_2][Tf_2N]_2$: TBACl

Complex/mixture	T_m[a] (°C)	η_{dyn}[a,b] (10^{-3} Pa s)	ρ[a,b] (10^3 kg m^{-3})	Mg(II) concentration[a,b] (mol dm^{-3})
$[Mg(G1)_3][Tf_2N]_2$	92	n.d.	n.d.	n.d.
$[Mg(G2)_2][Tf_2N]_2$	155	n.d.	n.d.	n.d.
$[Mg(G3)_2][Tf_2N]_2$	31	131	1.43	1.52
$[Mg(G1)_3][Tf_2N]_2$: TBACl 1 : 1	n.d.	97	1.29	1.14
$[Mg(G3)_2][Tf_2N]_2$: TBACl 1 : 1	n.d.	64	1.26	1.03

[a] n.d.: not determined. [b] Measured at 80 °C.

 This journal is © The Royal Society of Chemistry 2020

Open Access Article. Published on 18 November 2020. Downloaded on 12/6/2025 10:29:05 AM.
This article is licensed under a Creative Commons Attribution-NonCommercial 3.0 Unported Licence.

measured on a Lovis 2000 ME rolling-ball microviscometer and a DMA 4500 M density meter, respectively. In order to avoid contact with air, the samples were transferred from their sealed argon-filled containers to a syringe and subsequently injected into the capillaries or density chamber of the device. The temperature during both the viscosity and density measurements was controlled by the internal thermostat of the device. FT-Raman spectra were recorded between 3500 cm^{-1} and 50 cm^{-1} on a Bruker Vertex 70 spectrometer with a Ram II Raman module and a liquid-nitrogen-cooled germanium diode detector. Each measurement consisted of 64 scans at a resolution of 2 cm^{-1} with a 1064.38 nm laser (Nd:YAG) at a power of 250 mW. Samples were measured inside 2 mL glass vials that were filled inside the glovebox and subsequently closed with airtight screw caps. All the electrochemical measurements were performed inside an argon-filled glovebox with water and oxygen concentrations below 1 ppm. Cyclic voltammograms (CVs) and galvanostatic depositions were measured using an Autolab PGSTAT302N potentiostat and Nova 2.1 software. The working electrode for CV was a polished platinum disk electrode ($\phi = 0.5$ mm), unless stated otherwise, the counter electrode was magnesium metal ribbon (≥99.5%, Sigma Aldrich) and the scan rate was 50 mV s^{-1}. The reference electrode consisted of a platinum wire, submerged in a solution of ferrocene (Fc) and ferrocenium hexafluorophosphate ($FcPF_6$) (5 mmol L^{-1} each) in the ionic liquid *N*-butyl-*N*-methylpyrrolidinium bis(trifluoromethylsulfonyl)imide ([BMP][Tf_2N]), contained inside a fritted glass tube. For some other CV measurements and the chronopotentiometry experiments, other working electrodes were used, such as silicon wafers, coated with 100 nm platinum or gold. The coated wafers were also used as substrate for the galvanostatic depositions. The electrolytes were heated at 80 °C in a copper block on a hotplate equipped with a thermocouple for temperature control. Scanning electron microscopy (SEM) was performed on an XL30 FEG scanning electron microscope. Electrodepositions were made on gold- or platinum-coated silicon wafers and were thoroughly rinsed with anhydrous monoglyme and allowed to dry at ambient glovebox conditions before they were attached to the SEM sample holder with conductive carbon tape. Energy dispersive X-ray fluorescence (EDX) analysis was performed in the same setup with TEAM software. The acceleration voltage was 20 kV for both imaging and EDX. X-ray diffraction patterns were recorded on a Seifert 3003 T/T X-ray diffractometer in a 2θ range of 10°–90°, using a Cu Kα X-ray source. The samples were rotated during the measurement to ensure a consistent result. The reference codes for assignment are 01-071-6543 for magnesium and 01-087-0642 for platinum.

Synthesis and characterization data of complexes

[Mg(G1)$_3$][Tf$_2$N]$_2$. A mixture of $Mg(Tf_2N)_2$ (1.001 g, 1.712 mmol) and G1 (0.458 g, 5.082 mmol) was stirred in a closed glass vial at 100 °C until complete dissolution of the solid. Upon cooling, the mixture crystallized out to give $[Mg(G1)_3][Tf_2N]_2$ (1.459 g, 1.710 mmol, 100% yield) as a colorless crystalline solid. (FT-Raman shifts/cm^{-1}): 2968, 2865, 2739, 1480, 1453, 1357, 1334, 1284, 1244, 1140, 1094, 1019, 883, 826, 742, 593, 572, 553, 403, 341, 298, 279, 169, 122. Melting point: 92 °C.

[Mg(G2)$_2$][Tf$_2$N]$_2$. A mixture of $Mg(Tf_2N)_2$ (1.008 g, 1.724 mmol) and G2 (0.460 g, 3.428 mmol) was stirred in a closed glass vial at 160 °C until complete dissolution of the solid. Upon cooling, the mixture crystallized out to give $[Mg(G2)_2][Tf_2N]_2$ (1.468 g, 1.721 mmol, 100% yield) as a colorless crystalline solid. (FT-Raman shifts/cm^{-1}): 2968, 2912, 2861, 2796, 2754, 1482, 1453, 1401, 1353, 1335, 1281, 1244, 1206, 1128, 1108, 1062, 1025, 957, 891, 837, 794, 742, 632, 592, 572, 557, 399, 384, 341, 327, 314, 298, 279, 167, 122. Melting point: 155 °C.

[Mg(G3)$_2$][Tf$_2$N]$_2$. A mixture of $Mg(Tf_2N)_2$ (1.005 g, 1.719 mmol) and G3 (0.611 g, 3.428 mmol) was stirred in a closed glass vial at 100 °C until complete dissolution of the solid. Upon cooling, the mixture crystallized out to give $[Mg(G3)_2][Tf_2N]_2$ (1.616 g, 1.717 mmol, 100% yield) as a colorless crystalline solid. (FT-Raman shifts/cm^{-1}): 2964, 2911, 2850, 2792, 2765, 1477, 1451, 1404, 1354, 1336, 1305, 1281, 1267, 1244, 1199, 1139, 1107, 1061, 1024, 926, 886, 845, 799, 742, 632, 592, 572, 553, 516, 399, 341, 327, 314, 298, 279, 167, 121. Melting point: 31 °C. Dynamic viscosity (80 °C): 131 mPa s.

Results and discussion

Synthesis and physicochemical properties

The SILs were prepared by mixing $Mg(Tf_2N)_2$ with a stoichiometric amount of the ligands, monoglyme (G1), diglyme (G2) and triglyme (G3), in a closed vessel and stirring under heating until a homogeneous liquid was obtained. Upon cooling, the mixtures crystallized as colorless solids. The structural formulae of the anion and ligands can be found in Fig. 1.

The 1 : 1 mixtures were prepared in a similar way from the pure SILs and TBACl. The melting points of the pure complexes are given in Table 1, as well as the dynamic viscosity, density and magnesium concentration of the complexes and mixtures that were liquid at 80 °C. The melting points of $[Mg(G1)_3][Tf_2N]_2$ and $[Mg(G2)_2][Tf_2N]_2$ were higher than the maximum operational temperature of the density/viscosity meter (90 °C), so

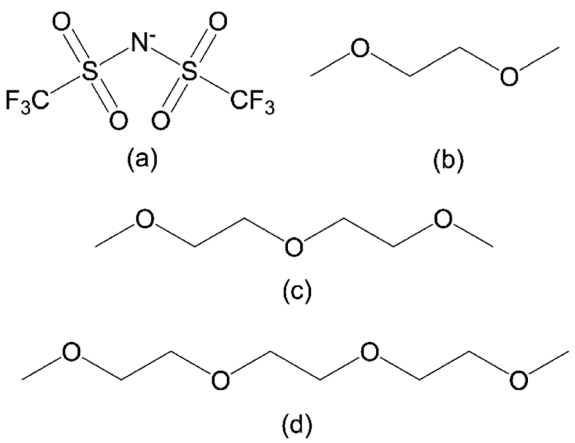

Fig. 1 Structural formulas of the anion and ligands used in this work: (a) bis(trifluoromethylsulfonyl)imide (Tf_2N^-), (b) monoglyme (G1), (c) diglyme (G2), and (d) triglyme (G3).

Open Access Article. Published on 18 November 2020. Downloaded on 12/6/2025 10:29:05 AM.
This article is licensed under a Creative Commons Attribution-NonCommercial 3.0 Unported Licence.

these properties could not be determined in this case. The mixtures of the SILs and TBACl did not exhibit a sharp transition from the solid to the liquid state, so a melting point could not be reported. The detailed synthesis and characterization data can be found in the Experimental section.

The melting points of $[Mg(G1)_3][Tf_2N]_2$ and $[Mg(G2)_2][Tf_2N]_2$ are high, primarily due to the high charge density of the six-coordinate solvated Mg(II) ions, which have a strong electrostatic attraction to the anions. In contrast, the melting point of $[Mg(G3)_2][Tf_2N]_2$ is close to room temperature. Thermogravimetric analysis (TGA) of the complexes and ligands also shows significantly different behavior of $[Mg(G3)_2][Tf_2N]_2$ compared to $[Mg(G1)_3][Tf_2N]_2$ and $[Mg(G2)_2][Tf_2N]_2$ (Fig. 2). The volatility of the glymes is significantly less for the magnesium complexes compared to the pure samples, in particular for $[Mg(G2)_2][Tf_2N]_2$ and $[Mg(G3)_2][Tf_2N]_2$.

However, evaporation for $[Mg(G3)_2][Tf_2N]_2$ occurs at a slightly higher rate than for $[Mg(G2)_2][Tf_2N]_2$, which is opposite to the trend expected from the chelate effect. These different physicochemical properties of $[Mg(G3)_2][Tf_2N]_2$ can be explained by a difference in its solvation structure. The solvate structures of the SILs were further studied by Raman spectroscopy and compared with previously reported literature data. The speciation of Mg(II) ions in G1 has already been extensively studied by Salama *et al.* using single crystal X-ray diffraction, Raman spectroscopy and ^1H and ^{13}C nuclear magnetic resonance spectroscopy.[31] The Mg(II) ions are completely encaged by three G1 molecules resulting in a solvent separated ion pair (SSIP) solvate structure. This can be observed in the compared Raman spectra of $[Mg(G1)_3][Tf_2N]_2$, pure G1 and pure $Mg(Tf_2N)_2$ in the 900–720 cm^{-1} range (Fig. S1†). The bands at 822 and 850 cm^{-1}, which correspond to the coupled CH_2 rocking ($r(CH_2)$) and COC stretching (ν(COC)) modes of uncoordinated G1 molecules,[26] are completely absent in the spectrum of $[Mg(G1)_3][Tf_2N]_2$. Instead, two new bands are observed around 883 and 869 cm^{-1}, shifted to higher wavenumbers, which correspond to the same modes observed for glymes that are coordinated to Mg(II) ions.[29] In the spectrum of $[Mg(G1)_3][Tf_2N]_2$, another band is observed at 742 cm^{-1}, which corresponds to the expansion–contraction mode of an uncoordinated Tf_2N^- anion.[29] The slight shoulder in this band at higher wavenumbers might be indicative for the minor presence of contact ion pairs (CIPs). In comparison, this band is shifted significantly towards higher wavenumbers for pure $Mg(Tf_2N)_2$, which is expected because the anions are the only species that can coordinate to the Mg(II) cations. It is expected that $[Mg(G2)_2][Tf_2N]_2$ also has a SSIP solvate structure and the Mg(II) ions are encaged by two G2 molecules resulting in a six-coordinate $[Mg(G2)_2]^{2+}$ cation. This is supported by the compared Raman spectra of $[Mg(G2)_2][Tf_2N]_2$ and pure G2 (Fig. 3).

The bands corresponding to uncoordinated G2 are located at 807 and 852 cm^{-1} but are not present in the spectrum of $[Mg(G2)_2][Tf_2N]_2$. Furthermore, the expansion–contraction band of Tf_2N^- is located at 742 cm^{-1}, and is symmetric (no shoulder), confirming the SSIP solvate structure for this SIL.[29] Similarly, the SSIP structure is also observed for $[Mg(G3)_2][Tf_2N]_2$, based on the Raman spectrum (Fig. S2†). This is also supported by the solvation study reported by Kimura *et al.*, which suggests that magnesium salts completely dissociate to form $[Mg(G3)_2]^{2+}$ complex cations when dissolved in triglyme.[32] However, as opposed to sodium SILs, where the G3 ligands adopt an eight-coordinate conformation around the sodium

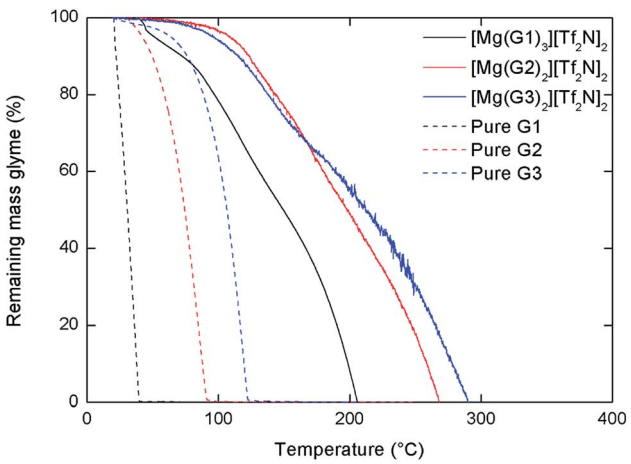

Fig. 2 Dynamic TGA curves of $[Mg(G1)_3][Tf_2N]_2$, $[Mg(G2)_2][Tf_2N]_2$ and $[Mg(G3)_2][Tf_2N]_2$ (full lines), and pure glymes (dashed lines), recorded at a heating rate of 5 °C min^{-1} under a N_2 atmosphere of 60 mL min^{-1}.

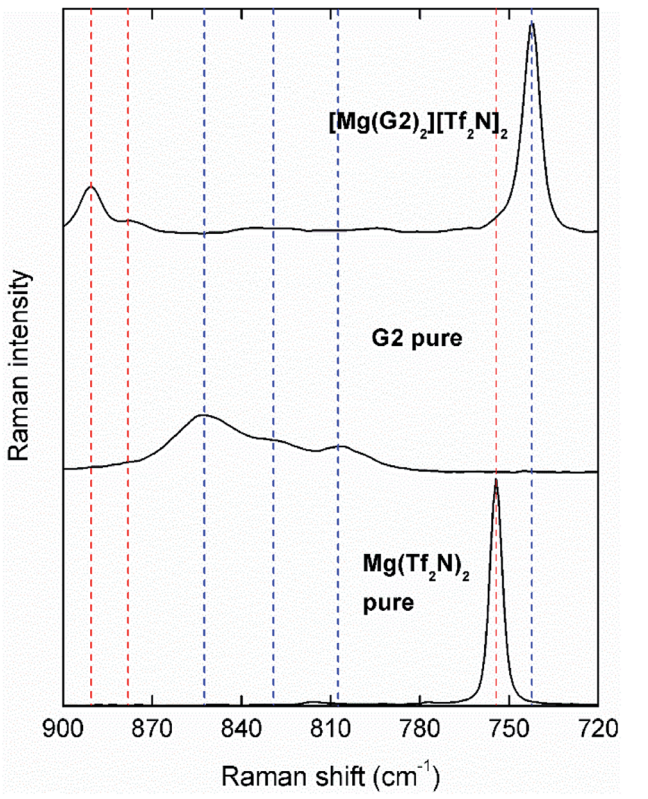

Fig. 3 Raman spectra of $[Mg(G2)_2][Tf_2N]_2$ (top), pure G2 (middle), and $Mg(Tf_2N)_2$ (bottom) in the range from 900 cm^{-1} to 720 cm^{-1}. The red and blue dashed lines are a visual aid to show the bands corresponding to coordinated and uncoordinated ligands/anions, respectively.

This journal is © The Royal Society of Chemistry 2020

Open Access Article. Published on 18 November 2020. Downloaded on 12/6/2025 10:29:05 AM.
This article is licensed under a Creative Commons Attribution-NonCommercial 3.0 Unported Licence.

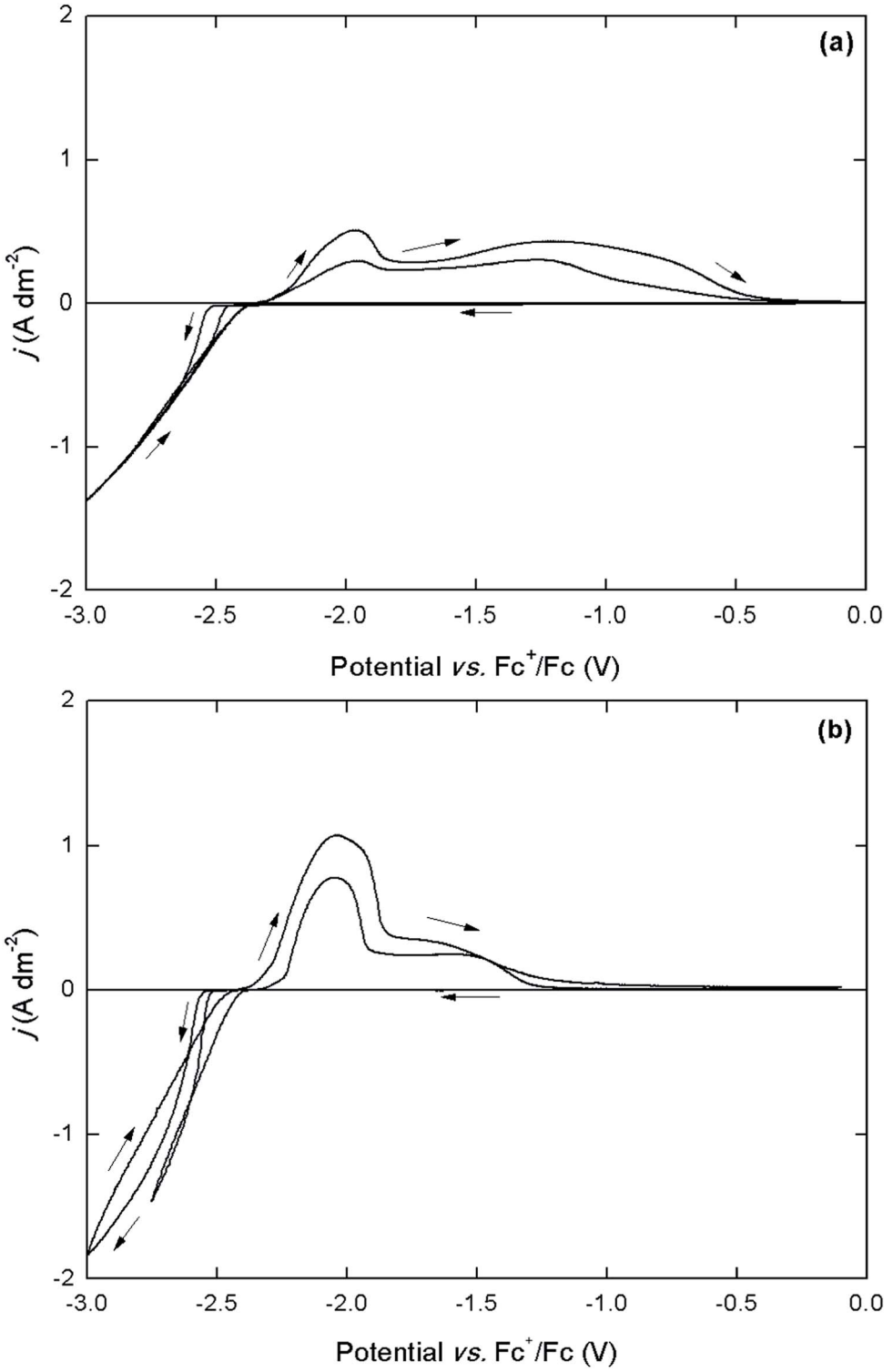

Fig. 4 Cyclic voltammograms (first cycle) of $[Mg(G1)_3][Tf_2N]_2$: TBACl 1 : 1 (a), and $[Mg(G3)_2][Tf_2N]_2$: TBACl 1 : 1 (b) at different cathodic vertex potentials, recorded on a platinum disk working electrode at 80 °C. The counter electrode was magnesium, the reference electrode was Fc^+/Fc in $[BMP][Tf_2N]$, and the scan rate was 50 mV s^{-1}. The arrows indicate the scan direction.

cations, a six-coordinate octahedral conformation is observed for $[Mg(G3)_2]^{2+}$.[26] In fact, an equilibrium occurs between a form where both G3 ligands are tridentate, and a form where one G3 ligand is bidentate and the other one tetradentate. This introduces more asymmetry in the crystal structure and decreases the average Mg–O bond strength, which results in a significantly

Open Access Article. Published on 18 November 2020. Downloaded on 12/6/2025 10:29:05 AM.
This article is licensed under a Creative Commons Attribution-NonCommercial 3.0 Unported Licence.

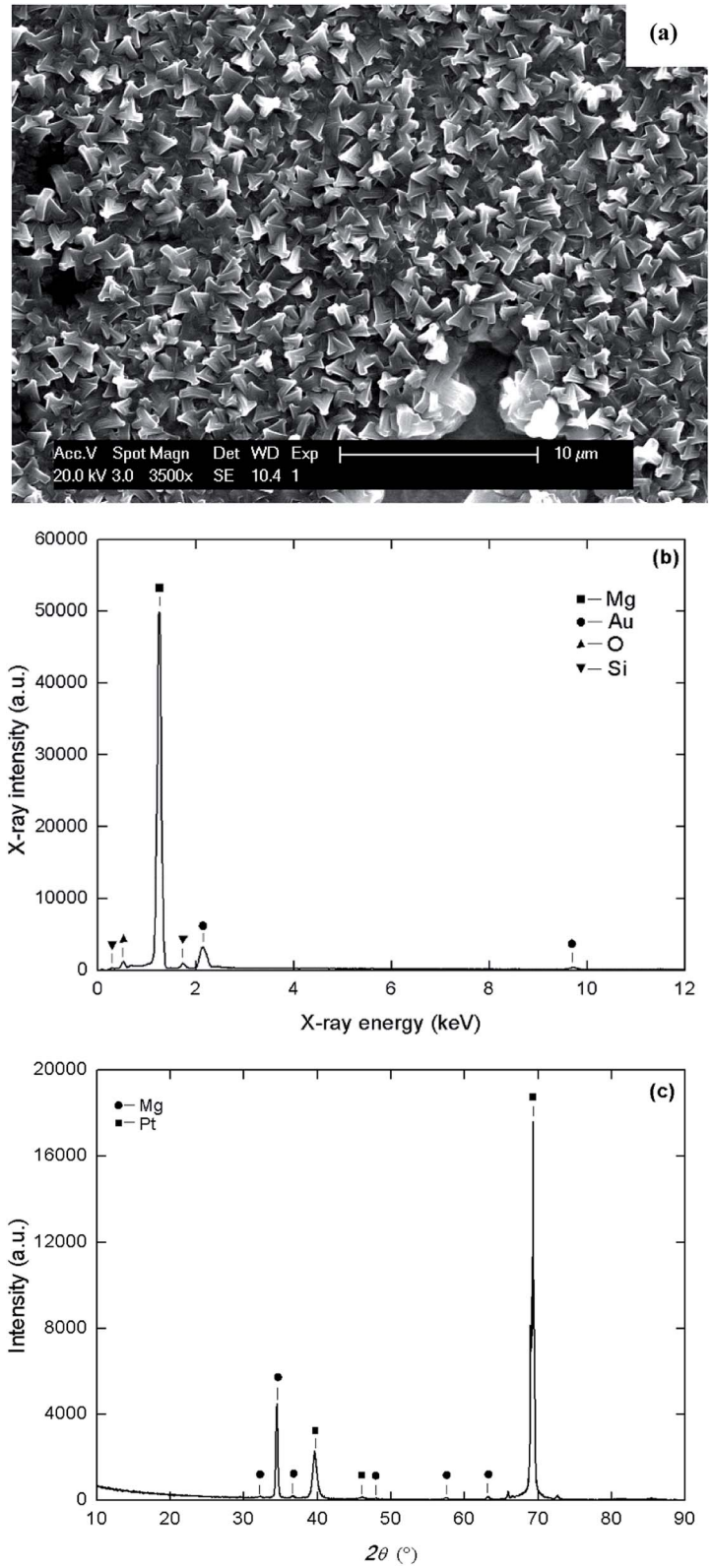

Fig. 5 SEM micrograph of an approx. 3 μm thick Mg deposit from $[Mg(G3)_2][Tf_2N]_2$: TBACl 1 : 1 at −1.0 A dm^{-2} on a gold-coated silicon wafer working electrode (a) and the EDX spectrum of this deposit, recorded at an acceleration voltage of 20 kV (b). (c) Depicts the XRD pattern of an approx. 30 μm thick magnesium layer deposited at −1.0 A dm^{-2} on a platinum-coated silicon wafer electrode. The reference codes for peak assignment are 01-071-6543 for Mg and 01-087-0642 for Pt.

 This journal is © The Royal Society of Chemistry 2020

Open Access Article. Published on 18 November 2020. Downloaded on 12/6/2025 10:29:05 AM.
This article is licensed under a Creative Commons Attribution-NonCommercial 3.0 Unported Licence.

lower melting point of $[Mg(G3)_2][Tf_2N]_2$ compared to the G1 and G2 SILs and also a lower thermal stability. A schematic representation of the SSIP solvate structure for the three SILs can be found in the ESI (Fig. S3).†

Electrodeposition and stripping of magnesium

For the electrochemical characterization of the SIL electrolytes, one mole equivalent of tetrabutylammonium chloride (TBACl) was added as a source of chloride ions, in order to achieve reversible magnesium deposition.[33] This had the additional benefit of lowering the viscosity of the electrolytes, while also maintaining a high Mg(II) concentration (Table 1). The mixtures of the SILs and TBACl were studied with cyclic voltammetry at 80 °C (Fig. 4).

Even though the melting point of pure $[Mg(G1)_3][Tf_2N]_2$ is above 80 °C, the 1 : 1 mixture with TBACl is completely molten at this temperature. The $[Mg(G2)_2][Tf_2N]_2$ mixture was not completely liquid, even at temperatures above 100 °C and was not studied further. In electrochemical experiments on magnesium electrodeposition, it is common to use a magnesium wire as a pseudo-reference electrode.[8–17] However, since magnesium easily forms insulating surface layers depending on the electrolyte composition, its reference potential is not very reliable when comparing different electrolytes, which can lead to wrong conclusions. This can be observed in Fig. S4,† where both the deposition and stripping onsets are shifted towards negative potentials *vs.* the Mg^{2+}/Mg pseudo-reference electrode. Instead, a real ferrocenium/ferrocene (Fc^+/Fc) reference electrode was used, where the reference solution (5 mM Fc^+/Fc in [BMP][Tf_2N]) was separated from the electrolyte by a glass frit (Fig. 4). In the negative scan direction, an abrupt negative current density is observed at approx. −2.6 V or −2.7 V *vs.* Fc^+/Fc for $[Mg(G1)_3][Tf_2N]_2$: TBACl 1 : 1 and $[Mg(G3)_2][Tf_2N]_2$: TBACl 1 : 1, respectively. This reduction corresponds to the deposition of magnesium metal, which is supported by the presence of a nucleation loop. The deposition current densities are high and do not reach a limiting value, owing to the high concentration of Mg(II) ions in these electrolytes. In the reverse scan, a stripping peak is observed, which consists of one relatively sharp peak at lower potentials, and a second broader peak at higher potentials. This unusual appearance of a double stripping peak has, to our knowledge, not been reported before for magnesium deposition. However, since the current density of both parts of the peak scales similarly with the cathodic vertex, they both seem to be related to the deposition process.

In order to further study the electrodeposition of magnesium in these electrolytes, galvanostatic deposits were prepared using gold- and platinum-coated silicon wafers as substrates. Fig. 5 shows a scanning electron micrograph of approx. 3 μm magnesium deposits on a gold-coated wafer (a), the corresponding energy-dispersive X-ray (EDX) spectrum (b) and the X-ray diffraction (XRD) pattern of a 30 μm deposit on a platinum-coated silicon wafer (c). The high Mg(II) concentration of these SIL-based electrolytes allowed to deposit at a high current density of −1.0 A dm^{-2}, which resulted in a rough plate-like morphology with inconsistent thickness and incomplete coverage of the substrate. In the EDX spectrum, the Kα line of magnesium is clearly observed as the most prominent peak. The peaks corresponding to the underlying gold and silicon layers of the substrate are much less intense, indicating that the deposit is thick. A minor peak corresponding to oxygen is also observed because the deposit was exposed to air during sample preparation, resulting in a thin surface layer of magnesium oxide. For the XRD analysis, a much thicker 30 μm deposit was required due to the intense signals associated with the underlying platinum layer at 39° and 68° 2θ. In the XRD pattern, the most prominent peak associated with pure magnesium metal is located at a 2θ value of 34°.

Because a double stripping peak is unusual for magnesium deposition, additional experiments were conducted on the $[Mg(G3)_2][Tf_2N]_2$: TBACl electrolytes in order to find an explanation for this phenomenon. The possibility of alloy formation was ruled out by measuring cyclic voltammograms on different working electrodes, namely platinum, gold and magnesium (Fig. S5†). The double stripping feature was clearly present for each working electrode material, even for pure magnesium metal. As a second possibility, the influence of the chloride-to-magnesium ratio was investigated. As speculated by Salama *et al.*, the presence of chloride ions can aid the magnesium deposition and stripping process in multiple ways.[33]

Fig. 6a depicts cyclic voltammograms measured in the neat SIL $[Mg(G3)_2][Tf_2N]_2$ and mixtures with TBACl in various ratios. The deposition of magnesium metal starts around −2.6 V *vs.* Fc^+/Fc for all the electrolytes. For the neat SIL, the stripping peak was only observed at a large overpotential, similarly to the observations for dilute $Mg(Tf_2N)_2$–G4 electrolytes.[29] When TBACl was added to the electrolytes, a second sharper peak at more negative potentials appeared in the voltammograms. Furthermore, as the ratio of TBACl to the SIL was increased, the size of this peak significantly increased, both in width and height. The broader part of the stripping peak was shifted to the cathodic side until it almost disappeared for the $[Mg(G3)_2][Tf_2N]_2$: TBACl 2 : 3 electrolyte. In the chronopotentiometry experiments, the electrodeposition of magnesium occurs at a constant potential of approx. −3.0 V *vs.* Fc^+/Fc. When a positive current is applied on this deposit several anodic processes are observed at different potential plateaus. For the neat $[Mg(G3)_2][Tf_2N]_2$ electrolyte, the first plateau is observed around −1.0 V *vs.* Fc^+/Fc, corresponding to the broad stripping peak at large overpotential in the CVs. The second plateau is most likely related to the anodic decomposition of the electrolyte, judging from the highly positive potential (>+2.0 V *vs.* Fc^+/Fc). As the chloride concentration in the electrolytes is increased, the overall stripping overpotential is decreased, and another plateau is observed corresponding to the sharp part of the stripping peak. These results strongly suggest that the stripping of magnesium metal is governed by two competing reactions, where the one at more negative potential involves chloride anions. Clearly, the presence of chloride anions in these electrolytes is essential to achieve efficient stripping of the deposited magnesium layers, as it lowers the stripping overpotential, but also significantly increases the reversibility of the magnesium deposition process, judging by the accompanying charge

Open Access Article. Published on 18 November 2020. Downloaded on 12/6/2025 10:29:05 AM.
This article is licensed under a Creative Commons Attribution-NonCommercial 3.0 Unported Licence.

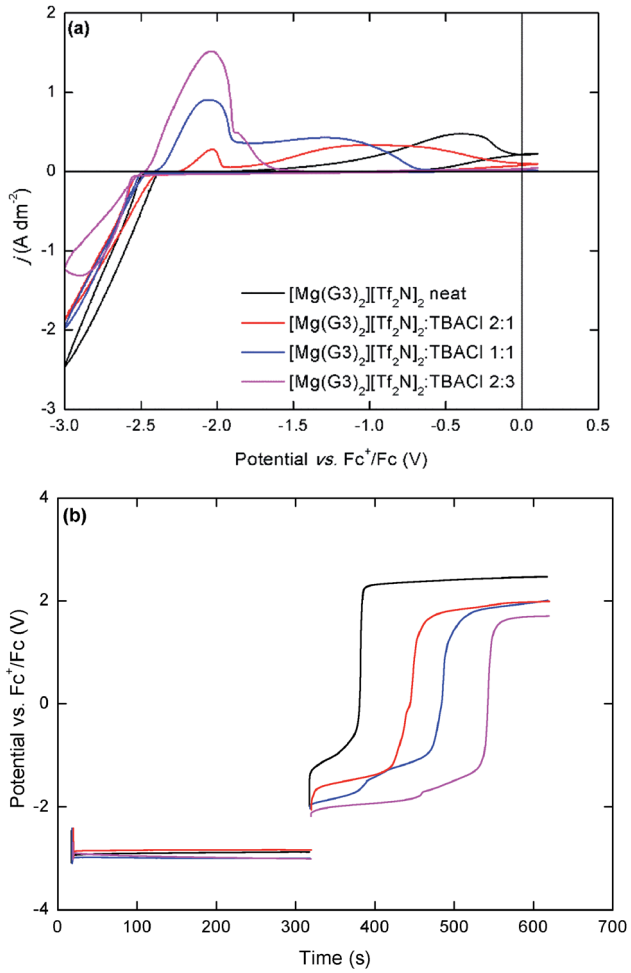

Fig. 6 (a) Cyclic voltammograms (first cycle) of $[Mg(G3)_2][Tf_2N]_2$: TBACl in various ratios, recorded on a platinum disk working electrode at 80 °C. The counter electrode was magnesium, the reference electrode was Fc^+/Fc in $[BMP][Tf_2N]$, and the scan rate was 50 mV s^{-1}. (b) Chronopotentiometry of the same $[Mg(G3)_2][Tf_2N]_2$: TBACl mixtures, recorded on a platinum-coated silicon wafer electrode (approx. surface area = 0.002 dm^{-2}). Magnesium was galvanostatic deposited at −0.3 A dm^{-2} for 300 s, followed by 300 s galvanostatic stripping at +0.3 A dm^{-2}.

vs. time plots (Fig. S6†). Probably, when the chloride concentration is low, the magnesium deposit surface is quickly passivated and decomposition of the electrolyte is observed instead.

It is also worth to note that, in these electrolytes, the use of a real Fc^+/Fc reference electrode allowed us to determine that the magnesium deposition potential is actually independent of the chloride concentration of the electrolyte, whereas the stripping peak onset potential is highly dependent on the chloride concentration. When a magnesium pseudo-reference electrode was used, a seemingly different result was found (Fig. S7†). Here, the magnesium deposition potential seemed so shift strongly to more negative potentials as the chloride concentration was decreased, while the onset of the stripping peaks remained approximately at the same potential. This result supports the hypothesis that the adsorption of chloride ions on the magnesium surface and/or the formation of different complex species plays a major role in the magnesium stripping mechanism.[33] However, further investigation of this mechanism is beyond the scope of this work.

Conclusion

Three new magnesium-containing solvate ionic liquids, $[Mg(G1)_3][Tf_2N]_2$, $[Mg(G2)_2][Tf_2N]_2$ and $[Mg(G3)_2][Tf_2N]_2$ are reported. All three SILS adopt a solvent separated ion pair solvate structure, as confirmed by Raman spectroscopy. When $[Mg(G1)_3][Tf_2N]_2$ and $[Mg(G3)_2][Tf_2N]_2$ are mixed with tetrabutylammonium chloride, highly concentrated non-volatile electrolytes are obtained that allow for electrodeposition and stripping of magnesium metal at high current densities (>1.0 A dm^{-2}). It was found that the presence of chloride anions has no significant influence on the magnesium deposition process, but plays an important role in the stripping process by decreasing the stripping overpotential and increasing the reversibility.

Conflicts of interest

There are no conflicts to declare.

Acknowledgements

The authors thank the KU Leuven for financial support (project KP/14/005). The research was supported by the European Research Council (ERC) under the European Union's Horizon 2020 Research and Innovation Programme: Grant Agreement 694078 – Solvometallurgy for critical metals (SOLCRIMET).

References

1 P. Canepa, G. Sai Gautam, D. C. Hannah, R. Malik, M. Liu, K. G. Gallagher, K. A. Persson and G. Ceder, *Chem. Rev.*, 2017, **117**, 4287–4341, DOI: 10.1021/acs.chemrev.6b00614.
2 R. Mohtadi and F. Mizuno, *Beilstein J. Nanotechnol.*, 2014, **5**, 1291–1311, DOI: 10.3762/bjnano.5.143.
3 C. Ling, D. Banerjee and M. Matsui, *Electrochim. Acta*, 2012, **76**, 270–274, DOI: 10.1016/j.electacta.2012.05.001.
4 M. Jäckle and A. Groß, *J. Chem. Phys.*, 2014, **141**, 174710–174717, DOI: 10.1063/1.4901055.
5 Z. Lu, A. Schechter, M. Moshkovich and D. Aurbach, *J. Electroanal. Chem.*, 1999, **466**, 203–217, DOI: 10.1016/S0022-0728(99)00146-1.
6 E. M. Erickson, E. Markevich, G. Salitra, D. Sharon, D. Hirshberg, E. de la Llave, I. Shterenberg, A. Rozenman, A. Frimer and D. Aurbach, *J. Electrochem. Soc.*, 2015, **162**, A2424–A2438, DOI: 10.1149/2.0991704jes.
7 L. W. Gaddum and H. E. French, *J. Am. Chem. Soc.*, 1927, **49**, 1295–1299, DOI: 10.1021/ja01404a020.
8 J. Muldoon, C. B. Bucur, A. G. Oliver, T. Sugimoto, M. Matsui, H. S. Kim, G. D. Allred, J. Zajicek and Y. Kotani, *Energy Environ. Sci.*, 2012, **5**, 5941–5950, DOI: 10.1039/c2ee03029b.
9 Y. Guo, F. Zhang, J. Yang and F. Wang, *Electrochem. Commun.*, 2012, **18**, 24–27, DOI: 10.1016/j.elecom.2012.01.026.

This journal is © The Royal Society of Chemistry 2020

Open Access Article. Published on 18 November 2020. Downloaded on 12/6/2025 10:29:05 AM.
This article is licensed under a Creative Commons Attribution-NonCommercial 3.0 Unported Licence.

10 D. Aurbach, Z. Lu, A. Schechter, Y. Gofer, H. Gizbar, R. Turgeman, Y. Cohen, M. Moshkovich and E. Levi, *Nature*, 2000, **407**, 724–727, DOI: 10.1038/35037553.

11 D. Aurbach, Y. Gofer, Z. Lu, A. Schechter, O. Chusid, H. Gizbar, Y. Cohen, V. Ashkenazi, M. Moshkovic, R. Turgeman and E. Levi, *J. Power Sources*, 2001, **97–98**, 28–32, DOI: 10.1016/S0378-7753(01)00585-7.

12 D. Aurbach, H. Gizbar, A. Schechter, O. Chusid, H. E. Gottlieb, Y. Gofer and I. Goldberg, *J. Electrochem. Soc.*, 2002, **149**, A115–A121, DOI: 10.1149/1.1429925.

13 O. Tutusaus, R. Mohtadi, T. S. Arthur, F. Mizuno, E. G. Nelson and Y. V. Sevryugina, *Angew. Chem., Int. Ed.*, 2015, **54**, 7900–7904, DOI: 10.1002/anie.201412202.

14 R. E. Doe, R. Han, J. Hwang, A. J. Gmitter, I. Shterenberg, H. D. Yoo, N. Pour and D. Aurbach, *Chem. Commun.*, 2014, **50**, 243–245, DOI: 10.1039/c3cc47896c.

15 S.-Y. Ha, Y.-W. Lee, S. W. Woo, B. Koo, J.-S. Kim, J. Cho, K. T. Lee and N.-S. Choi, *ACS Appl. Mater. Interfaces*, 2014, **6**, 4063–4073, DOI: 10.1021/am405619v.

16 I. Shterenberg, M. Salama, H. D. Yoo, Y. Gofer, J.-B. Park, Y.-K. Sun and D. Aurbach, *J. Electrochem. Soc.*, 2015, **162**, A7118–A7128, DOI: 10.1149/2.0161513jes.

17 Y. Cheng, R. M. Stolley, K. S. Han, Y. Shao, B. W. Arey, N. M. Washton, K. T. Mueller, M. L. Helm, V. L. Sprenkle, J. Liu and G. Li, *Phys. Chem. Chem. Phys.*, 2015, **17**, 13307–13314, DOI: 10.1039/c5cp00859j.

18 N. Sa, B. Pan, A. Saha-Shah, A. A. Hubaud, J. T. Vaughey, L. A. Baker, C. Liao and A. K. Burrell, *ACS Appl. Mater. Interfaces*, 2016, **8**, 16002–16008, DOI: 10.1021/acsami.6b03193.

19 G. T. Cheek, W. E. O'Grady, S. Z. El Abedin, E. M. Moustafa and F. Endres, *J. Electrochem. Soc.*, 2008, **155**, D91–D95, DOI: 10.1149/1.2804763.

20 A. Kitada, Y. Kang, K. Matsumoto, K. Fukami, R. Hagiwara and K. Murase, *J. Electrochem. Soc.*, 2015, **162**, D389–D396, DOI: 10.1149/2.0731508jes.

21 T. Mandai, K. Yoshida, K. Ueno, K. Dokko and M. Watanabe, *Phys. Chem. Chem. Phys.*, 2014, **16**, 8761–8772, DOI: 10.1039/c4cp00461b.

22 G. Vanhoutte, N. R. Brooks, S. Schaltin, B. Opperdoes, L. van Meervelt, J.-P. Locquet, P. M. Vereecken, J. Fransaer and K. Binnemans, *J. Phys. Chem. C*, 2014, **118**, 20152–20162, DOI: 10.1021/jp505479x.

23 H. Moon, R. Tatara, T. Mandai, K. Ueno, K. Yoshida, N. Tachikawa, T. Yasuda, K. Dokko and M. Watanabe, *J. Phys. Chem. C*, 2014, **118**, 20246–20256, DOI: 10.1021/jp506772f.

24 K. Ueno, J. Murai, H. Moon, K. Dokko and M. Watanabe, *J. Electrochem. Soc.*, 2017, **164**, A6088–A6094, DOI: 10.1149/2.0121701jes.

25 S. Terada, H. Susa, S. Tsuzuki, T. Mandai, K. Ueno, Y. Umebayashi, K. Dokko and M. Watanabe, *J. Phys. Chem. C*, 2016, **120**, 23339–23350, DOI: 10.1021/acs.jpcc.5b09779.

26 P. Geysens, V. Shankar Rangasamy, S. Thayumanasundaram, K. Robeyns, L. van Meervelt, J.-P. Locquet, J. Fransaer and K. Binnemans, *J. Phys. Chem. B*, 2018, **122**, 275–289, DOI: 10.1021/acs.jpcb.7b10158.

27 S. Tsuzuki, T. Mandai, S. Suzuki, W. Shinoda, T. Nakamura, T. Morishita, K. Ueno, S. Seki, Y. Umebayashi, K. Dokko and M. Watanabe, *Phys. Chem. Chem. Phys.*, 2017, **19**, 18262–18272, DOI: 10.1039/c7cp02779f.

28 K. Hashimoto, S. Suzuki, M. L. Thomas, T. Mandai, S. Tsuzuki, K. Dokko and M. Watanabe, *Phys. Chem. Chem. Phys.*, 2018, **20**, 7998–8007, DOI: 10.1039/c7cp08367j.

29 S. Terada, T. Mandai, S. Suzuki, S. Tsuzuki, K. Watanabe, Y. Kamei, K. Ueno, K. Dokko and M. Watanabe, *J. Phys. Chem. C*, 2016, **120**, 1353–1365, DOI: 10.1021/acs.jpcc.5b09779.

30 Y. Gofer, O. Chusid, H. Gizbar, Y. Viestfrid, H. E. Gottlieb, V. Marks and D. Aurbach, *Electrochem. Solid-State Lett.*, 2006, **9**, A257–A260, DOI: 10.1149/1.2186003.

31 M. Salama, I. Shterenberg, H. Gizbar, N. N. Eliaz, M. Kosa, K. Keinan-Adamsky, M. Afri, L. J. W. Shimon, H. E. Gottlieb, D. T. Major, Y. Gofer and D. Aurbach, *J. Phys. Chem. C*, 2016, **120**, 19586–19594, DOI: 10.1021/acs.jpcc.6b07733.

32 T. Kimura, K. Fujii, Y. Sato, M. Morita and N. Yoshimoto, *J. Phys. Chem. C*, 2015, **119**, 18911–18917, DOI: 10.1021/acs.jpcc.5b04626.

33 M. Salama, I. Shterenberg, L. J. W. Shimon, K. Keinan-Adamsky, M. Afri, Y. Gofer and D. Aurbach, *J. Phys. Chem. C*, 2017, **121**, 24909–24918, DOI: 10.1021/acs.jpcc.7b05452.